

Three-dimensional magnetic reconnection in complex multiple X-point configurations in an ancient solar-lunar terrestrial system

Xiang-Lei He(何向磊), Ao-Hua Mao(毛傲华), Meng-Meng Sun(孙萌萌), Ji-Tong Zou(邹继同), and Xiao-Gang Wang(王晓钢)

Citation: Chin. Phys. B, 2024, 33 (**3**): 035202. DOI: 10.1088/1674-1056/ad0b02
Journal homepage: http://cpb.iphy.ac.cn; http://iopscience.iop.org/cpb

What follows is a list of articles you may be interested in

Effect of the magnetization parameter on electron acceleration during relativistic magnetic reconnection in ultra-intense laser-produced plasma

Qian Zhang(张茜), Yongli Ping(平永利), Weiming An(安维明), Wei Sun(孙伟), and Jiayong Zhong(仲佳勇)
Chin. Phys. B, 2022, 31 (**6**): 065203. DOI: 10.1088/1674-1056/ac3397

Electron acceleration during magnetic islands coalescence and division process in a guide field reconnection

Shengxing Han(韩圣星), Huanyu Wang(王焕宇), and Xinliang Gao(高新亮)
Chin. Phys. B, 2022, 31 (**2**): 025202. DOI: 10.1088/1674-1056/ac21c0

Spontaneous growth of the reconnection electric field during magnetic reconnection with a guide field: A theoretical model and particle-in-cell simulations

Kai Huang(黄楷), Quan-Ming Lu(陆全明), Rong-Sheng Wang(王荣生), Shui Wang(王水)
Chin. Phys. B, 2020, 29 (**7**): 075202. DOI: 10.1088/1674-1056/ab8da0

Basic features of the multiscale interaction between tearing modes and slab ion-temperature-gradient modes

L Wei(魏来), Z X Wang(王正汹), J Q Li(李继全), Z Q Hu(胡朝清), Y Kishimoto(岸本泰明)
Chin. Phys. B, 2019, 28 (**12**): 125203. DOI: 10.1088/1674-1056/ab5437

Formation of electron depletion layer and parallel electric field in the separatrix region of anti-parallel magnetic reconnection

Zisheng Li(李子圣), Huanyu Wang(王焕宇), Xinliang Gao(高新亮)
Chin. Phys. B, 2019, 28 (**7**): 075203. DOI: 10.1088/1674-1056/28/7/075203

Three-dimensional magnetic reconnection in complex multiple X-point configurations in an ancient solar–lunar terrestrial system

Xiang-Lei He(何向磊)[1], Ao-Hua Mao(毛傲华)[1,2,†], Meng-Meng Sun(孙萌萌)[1], Ji-Tong Zou(邹继同)[1], and Xiao-Gang Wang(王晓钢)[1,2]

[1] *School of Physics, Harbin Institute of Technology, Harbin* 150001, *China*
[2] *Laboratory for Space Environment and Materials Science, Harbin Institute of Technology, Harbin* 150001, *China*

(Received 31 August 2023; revised manuscript received 5 November 2023; accepted manuscript online 9 November 2023)

Magnetic reconnection processes in three-dimensional (3D) complex field configurations have been investigated in different magneto-plasma systems in space, laboratory, and astrophysical systems. Two-dimensional (2D) features of magnetic reconnection have been well developed and applied successfully to systems with symmetrical property, such as toroidal fusion plasmas and laboratory experiments with an axial symmetry. But in asymmetric systems, the 3D features are inevitably different from those in the 2D case. Magnetic reconnection structures in multiple celestial body systems, particularly star–planet–Moon systems, bring fresh insights to the understanding of the 3D geometry of reconnection. Thus, we take magnetic reconnection in an ancient solar–lunar terrestrial magneto-plasma system as an example by using its crucial parameters approximately estimated already and also some specific applications in pathways for energy and matter transports among Earth, ancient Moon, and the interplanetary magnetic field (IMF). Then, magnetic reconnection of the ancient lunar–terrestrial magnetospheres with the IMF is investigated numerically in this work. In a 3D simulation for the Earth–Moon–IMF system, topological features of complex magnetic reconnection configurations and dynamical characteristics of magnetic reconnection processes are studied. It is found that a coupled lunar-terrestrial magnetosphere is formed, and under various IMF orientations, multiple X-points emerge at distinct locations, showing three typical magnetic reconnection structures in such a geometry, i.e., the X-line, the triple current sheets, and the A–B null pairs. The results can conduce to further understanding of reconnection physics in 3D for plasmas in complex magnetic configurations, and also a possible mechanism for energy and matters transport in evolutions of similar astrophysical systems.

Keywords: magnetic reconnection, multiple X-points, complex magneto-plasma system

PACS: 52.65.Kj, 94.30.cp, 96.12.Hg **DOI:** 10.1088/1674-1056/ad0b02

1. Introduction

Magnetic reconnection processes have been extensively observed and studies in space, astrophysical, and laboratory plasmas, particularly for explosive events such as solar flares, coronal mass ejections, magnetic storms and substorms, disruptive instabilities in toroidal fusion plasmas, etc.[1–6] An important development in magnetic reconnection studies is the fast reconnection dynamics in the collisionless regime[7–9] on a multiple scale as small as electron skin-depth.[10,11] On the other hand, progress is also made in the front of reconnection processes with complex field configurations, such as 2D multiple X-point reconnection models for space and laboratory plasmas,[12,13] and particularly 3D reconnection processes with multiple nulls and complex separatrix structures.[14–16] In fact, many celestial bodies[17–20] and galaxy clusters[21,22] in the universe have or ever had magnetic fields with various 3D configurations. Thus, for big planets (such as Jupiter and Saturn) with moons having remarkably durable magnetic fields, a typical 3D complex magnetic geometry can be formed in the moon–planet–IMF system. The energy/matters transport and evolution processes in such magnetic field configurations are essential to astrophysical research subjects. While magnetic reconnection physics around a single X-point has been extensively investigated and remarkable progress has been made,[1,23] however geometrical features and dynamical characteristics of 3D magneto-plasma systems with complex configurations are still open issues.

To our Earth–Moon–IMF system, although on the present lunar surface, only a negligible magnetic intensity of $<$ 0.2 nT,[24] $\sim 10^{-5}$ of that on the Earth, is detected, it is indicated that there had been a substantial lunar magnetic field billions of years (Ga) ago, by study of magnetized lunar rock samples.[25] It has been found that many Apollo samples carry significant remnant magnetization, indicating that the ancient lunar dynamos operating 4.25–2.5 billion years ago (Ga) had a substantial surface field of 5 μT–100 μT, comparable to that of today's Earth.[25] Particularly, because the Earth–Moon distance $\sim$ 4 Ga ago is shorter than the present value of $\sim$ 21.6 Earth-radius ($R_{\rm E}$),[26] the interaction would be stronger than today' value. Such Earth–Moon interactions were first studied in a model of parallel and antiparallel dipoles coupling in the Earth–Moon system,[27] where the ancient Moon was located 18 $R_{\rm E}$ away from the Earth. For simplification however, the IMF effect is reduced to a perfect paraboloid magne-

†Corresponding author. E-mail: aohuamao@hit.edu.cn

© 2024 Chinese Physical Society and IOP Publishing Ltd

topause surrounding the geomagnetosphere. The Earth–Moon fields then form various reconnection configurations in such a modeling geomagnetosphere to provide pathways between the Earth and the ancient Moon.

In this work, therefore, we develop the model into a 3D system open to the IMF environment of a typical moon–planet–IMF configuration to investigate complex geometry magnetic reconnection. The rest of this paper is organized as follows. The model and simulation setting are introduced and described in Section 2. Temporal evolutions of the Earth–Moon–IMF system in various IMF orientations, as well as features of magnetic reconnection for typical Earth–Moon relative positions, are revealed and analyzed in Section 3. The simulation mainly focus on representative reconnection processes of north or south IMF orientations with only brief descriptions for others. Then in Section 4, prospects and some conclusions are drawn and the prospects are also discussed.

2. Methods and simulation setups

The temporal evolution of the Earth–Moon magnetic field system in the IMF environment is modeled by a global 3D magnetohydrodynamics (MHD) model widely applied to space and astrophysical plasma physics, such as in coronal heating,[28] coronal mass ejection,[29] particularly geomagnetosphere–IMF coupling,[30–32] etc. A detailed description of the model and its numerical solver can be found in Ref. [33]. Characteristic parameters, such as the Earth–Moon distance ($D_{\rm EM} = 18R_{\rm E}$), fierce solar wind conditions due to the "faint young Sun",[34] and especially ancient Earth field and Moon field ~ 3 Ga–4 Ga ago[27] are selected in the simulation of this work. The magnetic field configurations are assumed to be generated by Earth–Moon dipoles, either parallel or anti-parallel in the north–south direction, in a steady IMF. And the respective intensities on Earth surface and Moon surface are approximately the same as $\sim B_{\rm surf} = 31.2$ μT, almost at a level on the present Earth surface.

Without loss of generality, the initial state can be assumed to be force-free with a constant pressure $p = p_{\rm sw} = n_{\rm sw}T_{\rm sw}$. The number density of the Earth's geomagnetosphere plasma is however approximately inversely proportional to the fourth power of the geocentric radius as[35]

$$\begin{aligned} &n_{\rm E} = n_0\left(\frac{r}{R_{\rm E}}\right)^{-4}, && r_{\rm b} \le r < r_{\rm a}, \\ &n_{\rm E} = n_{\rm sw}, && \text{otherwise}, \end{aligned} \tag{1}$$

with $r = (x^2+y^2+z^2)^{1/2}$, $n_0 = 10^4$ cm^{-3} and $n_{\rm sw} = 5$ cm^{-3} are the number densities of solar wind plasma and ionosphere plasma at $r \approx R_{\rm E}$ respectively, with r being the geocentric radius. Clearly, the r^{-4} distribution is extended only to $r_{\rm a} = 6.67R_{\rm E}$, slightly lower than the geostationary orbit, where $n_{\rm E}(r_{\rm a}) = n_{\rm sw} = 5\times10^{-4}n_0$. Meanwhile, we choose the inner simulation boundary at $r = r_{\rm b} = 3R_{\rm E}$, with $n_{\rm E}(r_{\rm b}) \approx 10^{-2}n_0$. It should be pointed out that at the Moon position of $r \sim 18R_{\rm E}$, the plasma density $n_{\rm M} \approx 0.1$ cm$^{-3} \ll n_{\rm sw}$ is obviously submerged in the background solar wind density $n_{\rm sw}$. Thus, under the force-free assumption for the initial distribution, the isothermal state $T = T_{\rm sw} =$ const. can be used, except for a small region of $r_{\rm b}(=3R_{\rm E}) \le r < r_{\rm a}(=6.67R_{\rm E})$ where $T(r)/T_{\rm sw} = (n_{\rm sw}/n_0)(r/R_{\rm E})^4$, with $T(r_{\rm a}) = T_{\rm sw}$, $T(r_{\rm b}) = T_{\rm sw}(r_{\rm b}/r_{\rm a})^4 \approx 4\times10^{-2}T_{\rm sw}$.

In the simulation, we rescale the variables into dimensionless quantities by characteristic parameters $R_{\rm E} = 6.37\times10^8$ cm for the length, as well as $B_0 = 0.312$ Gs $\approx B_{\rm surf}$, (1 Gs = 10^{-4} T), $\rho_0 = m_i n_0$ ($n_0 = 10^4$ cm^{-3}, the density at the ionosphere), and $p_0 = B_0^2/4\pi$ for the magnetic field, density, and pressure. Also, velocity, time, and current are normalized by the Alfven velocity $V_{\rm A} = B_0/\sqrt{4\pi\rho_0} = 6.8\times10^8$ cm·s^{-1}, Alfven time $\tau_{\rm A} = R_{\rm E}V_{\rm A}$, and $J_0 = cB_0/4\pi R_{\rm E}$. Besides, a low dimensionless resistivity is used as $\eta = 5\times10^{-4}$. Other solar wind parameters are $\boldsymbol{v}_{\rm sw} = (v_{\rm sw},0,0)$ with $v_{\rm sw} = 3\times10^7$ cm·s^{-1} $\approx 4.4\times10^{-2}V_{\rm A}$, $T_{\rm sw} = 2\times10^2$ eV $\approx 4\times10^{-4}T_0$ ($T_0 \equiv p_0/n_0$), and $B_{\rm IMF} = \pm4\times10^{-5}$ Gs $= \pm1.28\times10^{-4}B_0$, where $B_{\rm IMF}$ denotes the z-component of the IMF orientation.

Then, the density distribution (1) is rescaled dimensionally as

$$\begin{aligned} &n_{\rm E} = r^{-4}, && r_{\rm b} \le r < r_{\rm a}, \\ &n_{\rm E} = n_{\rm sw}, && \text{otherwise}, \end{aligned} \tag{2}$$

with $r_{\rm a} = 6.67$, $r_{\rm b} = 3$, and $n_{\rm sw} = 5\times10^{-4}$ ($T_{\rm sw} = 4\times10^{-4}$ and $p_{\rm sw} \approx 2\times10^{-7}$).

The simulation domain is a 3D cubic box of $L_{x0} \le x \le L_{x1}$, $-L_{y0} \le y \le L_{y0}$, and $-L_{z0} \le z \le L_{z0}$ with $L_{x0} = -70$, $L_{x1} = 30$, $L_{y0} = L_{z0} = 50$. And in general, the meridian plane of $y = 0$ is selected as a representative unless otherwise specified. The solar-wind/IMF flow into the domain through the boundary at $x = L_{x1}$. Thus, boundary conditions are adopted as a solar-wind/IMF driving boundary at $x = L_{x1}$, free boundaries at $x = L_{x0}$, $y = \pm L_{y0}$, and $z = \pm L_{z0}$. Besides, fixed boundary conditions are $r = 3R_{\rm E}$ as in Eq. (1), and 3 of lunar radius ($R_{\rm M}$) from the Moon center.

3. Results and discussion

Instead of two particular Moon positions at the noon and the midnight on the meridian plane in Ref. [27], in this work, we observe three typical local time (LT) positions of the Moon when it orbits the Earth, i.e., 0 LT (the midnight), 12 LT (the noon), and 6 LT (the dawn, symmetric to the dusk), as shown in Fig. 1. Contributions at the 18 LT position (the dusk) are the same as that at the 6 LT. Also, the geocentric solar ecliptic (GSE) coordinates are adopted with the origin in the center of the Earth.

The initial magnetic field configuration in the meridian plane of $y = 0$ is exhibited in Fig. 2. Taking the 0-LT case for example, the surface fields at the equator is assumed to be $B_0 \equiv |B_{\rm RE0}| = |B_{\rm RM0}|$,[27] where $B_{\rm RE0}$ is the surface field of the Earth and $B_{\rm RM0}$ is that of the Moon.

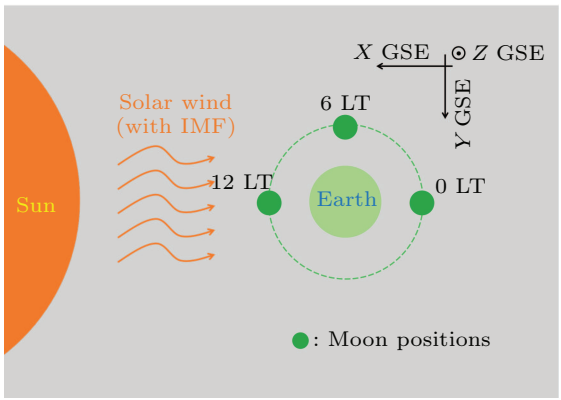


Fig. 1. Schematic diagram of the three representative positions in the simulation.

We then exhibit simulation results for three typical Moon positions with various Earth–Moon dipole alignments and different IMF orientations. For both antiparallel and parallel dipoles, quasi-steady-state configurations of the Earth–Moon system are reached in the 3D simulation for three typical Moon positions. In each case, the influence of the IMF orientation is also investigated. We first discuss reconnection features for the Moon at 0-LT and 12-LT positions, which are corresponding to midnight and noon, respectively, because of the similarity to the 2D geometry due to the symmetry about the meridian plane of $y = 0$. The reconnection process for the Moon at the 6-LT position (case dawn) is investigated in a full 3D picture. The case for the Moon at the 18-LT position (case dusk) is similar to the case dawn due to the mirror symmetry.

By analyzing the characteristics of magnetic nulls and separatrices, major features of magnetic reconnection in the Earth–Moon–IMF system, such as the current sheet and in-outflow structures, can be acquired. The temporal evolution and plasma-magnetic configurations of the system are then investigated in detail for various dipole alignments, IMF orientations, and relative positions of the Earth and the Moon.

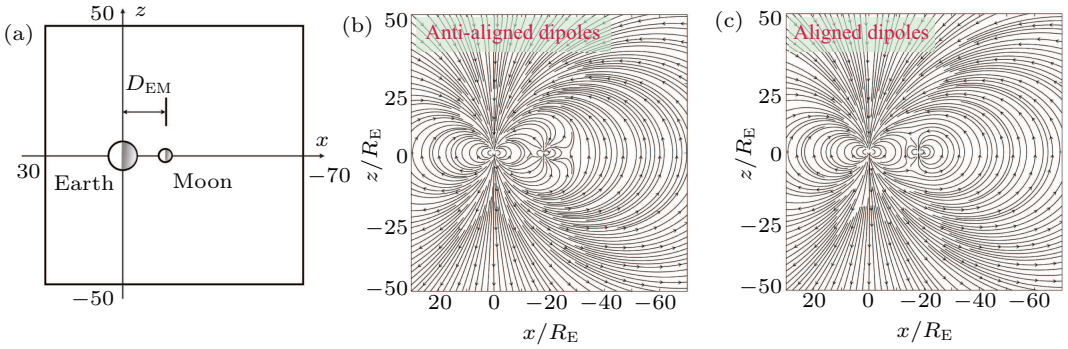


Fig. 2. (a) Cross-section of meridian plane for 0-LT case, and initial magnetic field distribution for (b) antiparallel dipoles and (c) parallel dipoles.

3.1. Magnetic reconnection for the Moon at 0-LT position

In order to clearly show the characteristics of reconnection configurations and plasma, we mainly describe the process in a 2D approximation.

Magnetic reconnection in the 2D geometry has been extensively studied.[1,36,37] Clearly, in the case midnight, the 2D projection onto the meridian is always of a 2D X-point geometry. The 3D simulations show that there are three typical reconnection configurations in the Earth–Moon system: (i) the X-line structure, (ii) the triple current sheet structure, and (iii) the A–B null pair structure. Each reconnection geometry is investigated in detail at a quasi-steady-state (QSS) with certain typical examples.

Now, we take a specific case for example. In Fig. 3, we plot QSS magnetospheric configurations on the meridian plane ($y = 0$), with antiparallel Earth–Moon diploes being in the southward IMF at 0 LT. A typical magnetosphere with a parabolic shape is formed and clearly observed by the dayside compression in the nightside drag of the IMF. Clearly, positioning behind the Earth, the Moon cannot affect dayside reconnection at the geomagnetopause. For a southward IMF, dayside geomagnetopause reconnection occurs on the subsolar point (B1 marked in Fig. 3(b)), in accordance with conventional observations as well as theoretical and numerical models without the lunar magnetic field. Nevertheless, in the geomagnetotail region, reconnection sites and features are totally changed. Instead of at the near-Earth or far neutral lines, with a significant lunar magnetic field, magnetic reconnection appears in more places between the Earth and the Moon, on the equatorial ($z = 0$) plane (B2 marked in Fig. 3(b)) and at the cusps of the Moon (B3 for the upper, marked in Fig. 3(b)).

Then, we first investigate reconnection features at the equatorial plane site and show them in detail in Fig. 4. It is found that by the reconnection current J_y (Fig. 4(a)) and the plasma flow $\boldsymbol{v}$ distribution (Fig. 4(b)) with the inflow component of v_x (Fig. 4(c)) and outflow component of v_z (Fig. 4(d), the features are very similar to those in conventional geomagnetotail reconnection with no lunar field.

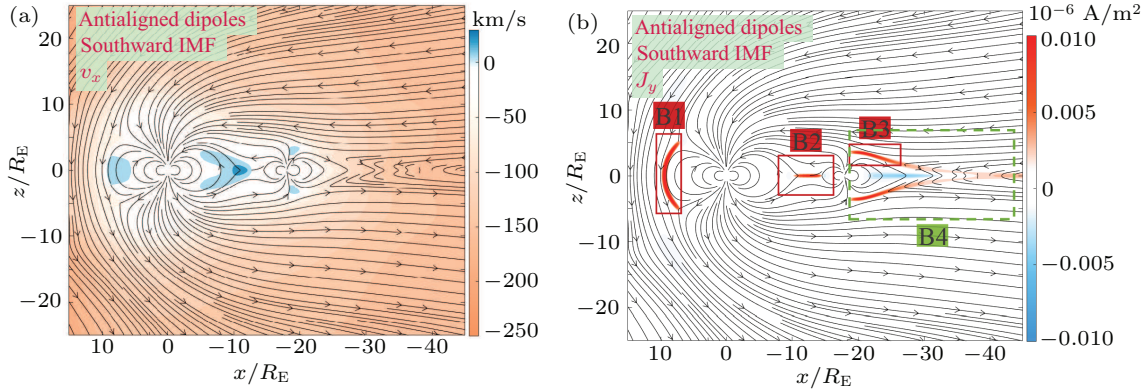


Fig. 3. QSS reconnection configurations in case midnight, with antiparallel dipoles and southward IMFs. Magnetic field lines (in black) projection, as well as (a) x-component velocity v_x and (b) y-component current density J_y (both by color bars) on the meridian plane.

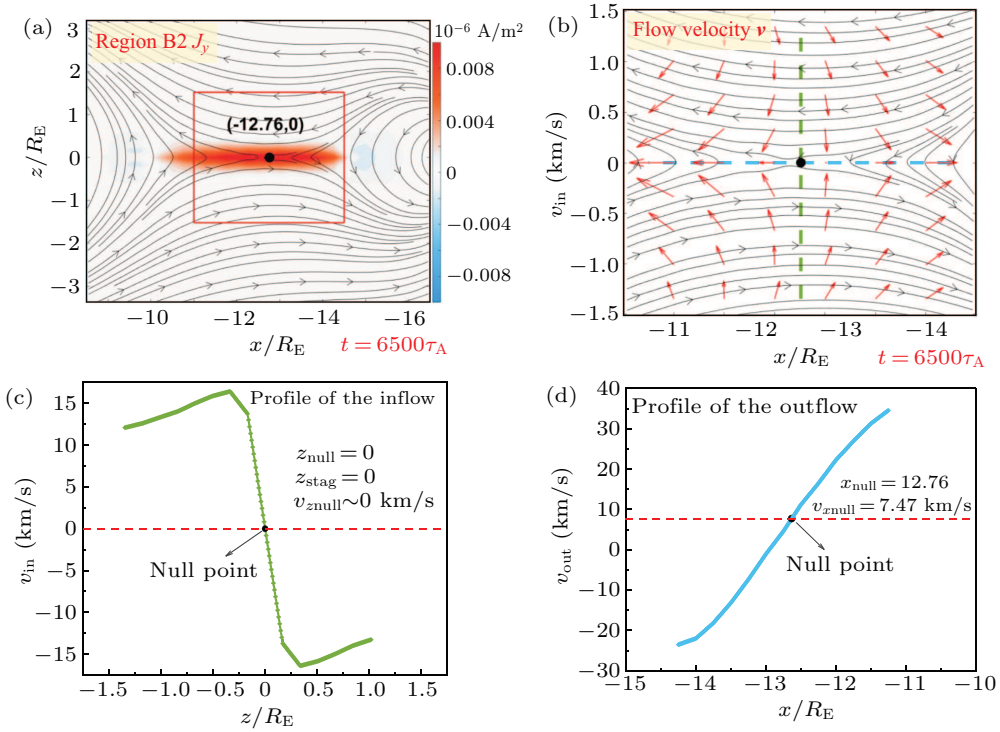


Fig. 4. Locally enlarged region around B2 marked in Fig. 3(c), for (a) reconnection current J_y and (b) plasma flow $\boldsymbol{v}$ distributions on equatorial ($z = 0$) plane; also for velocity profiles of (c) inflow and (d) outflow, along green and blue dotted lines marked in panel (b).

It can be found that the X-point (in 2D case) on the equatorial (z =0) plane is located at $(x,z) = (-12.76, 0)$, marked by the red dot in Figs. 4(a) and 4(b). A reconnection current J_y can be observed mostly distributed along the x direction to support the magnetic reconnection process. And the plasma flow forms a typical inflow–outflow structure as shown by arrows on the meridian plane. The moonward outflow can bring most of materials from the Earth's atmosphere to the Moon at a speed of $\sim$ 20 km/s, indicating that the reconnection has promotes the implantation of the lunar atmospheric proposed by Green.[27] Furthermore, one can calculate the reconnection rate by $|E_y| \approx 1.63 \times 10^{-6}$ at the X-point, for estimating the magnetic flux transport.

On the other hand, instead of a reconnection site in the lunar magnetotail on the equatorial plane, the other two reconnection sites of case midnight with antiparallel dipoles and southward IMFs appear in lunar cusps as shown in Fig. 5 for a local enlargement of the lunar magnetotail.

It can be seen that a triple current sheet configuration (of J_y) is formed with the $+y$ direction in two high latitude regions and the $-y$ direction near the equatorial $z = 0$. Such a triple current sheet structure has been observed in coronal helmet streamers[38] and advance tokamak scenarios with reversed magnetic shear.[39] Here, however, the magnetic configuration with triple current sheets in the Earth–Moon system is different from the previous one, for the central current sheet with neither magnetic separatrix nor reconnection. In the lunar cusp region as shown in Fig. 5(a), the closed lunar field lines are reconnected with the antiparallel magnetic field of the geomagnetosphere. Some newly reconnected field lines then turn to

open and sweep tailward with the plasma flow, others however become connecting both the Earth and the Moon. As a consequence, the nightside closed lines of the lunar field are kinked by the separatrices (marked by red lines in Fig. 5(b)) of cusp region reconnection. A distant neutral line might be formed as the central current sheet extends over $90R_E$ or even farther away. It is however far beyond the simulation domain and with little influence on the magnetic flux transfer discussed in this work.

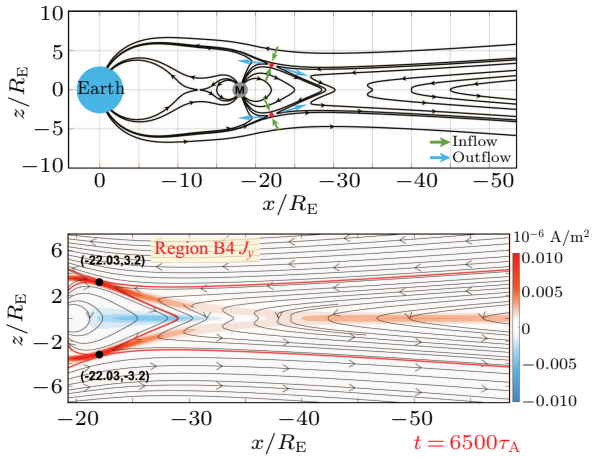


Fig. 5. (a) Schematic diagram for reconnection in lunar cusp region; (b) local enlargement of lunar magnetotail with upper cusp reconnection site marked as B4 in Fig. 3(b).

Unlike the antiparallel dipole geometry, reconnection in the parallel dipole geometry in case midnight occurs in the high latitude lunar cusp region, with no triple current sheet formed in the tail region.

Table 1. Antialigned dipoles at 0 LT.

IMF orientation	Reconnection site	Influences on the closed lunar magnetic flux
Southward	Geomagnetopause	
Southward	between Earth and Moon	increasing
Southward	lunar cusp regions	decreasing
Southward	lunar magnetotail	
Northward	Earth's cusp regions	
Northward	between Earth and Moon	increasing
Northward	lunar cusp regions	decreasing
Northward	lunar magnetotail	

Table 2. Aligned dipoles at 0 LT.

IMF orientation	Reconnection site	Influences on the closed lunar magnetic flux
Southward	geomagnetopause	
Southward	lunar cusp regions	decreasing
Southward	lunar magnetotail	increasing
Northward	Earth's cusp regions	
Northward	lunar cusp regions	decreasing
Northward	lunar magnetotail	increasing

Thus, magnetic reconnection processes with various dipole alignments and IMF orientations in case midnight are simulated and summarized, and the results are listed in Table 1, and the results of aligned dipoles are listed in Table 2. Their contributions to magnetic flux transport are discussed later.

3.2. Magnetic reconnection for Moon at 12-LT position

In comparison with case midnight, for case noon with the Moon at 12 LT, the magnetospheric shape is much more complicated as shown in Fig. 6. For the antiparallel dipoles, the magnetic reconnection site appears in the area between the Earth and the Moon (B2 marked in Fig. 6(b)), the lunar cusp region (B1 marked in Fig. 6(b)), and the geomagnetotail (B3 marked in Fig. 6(b)).

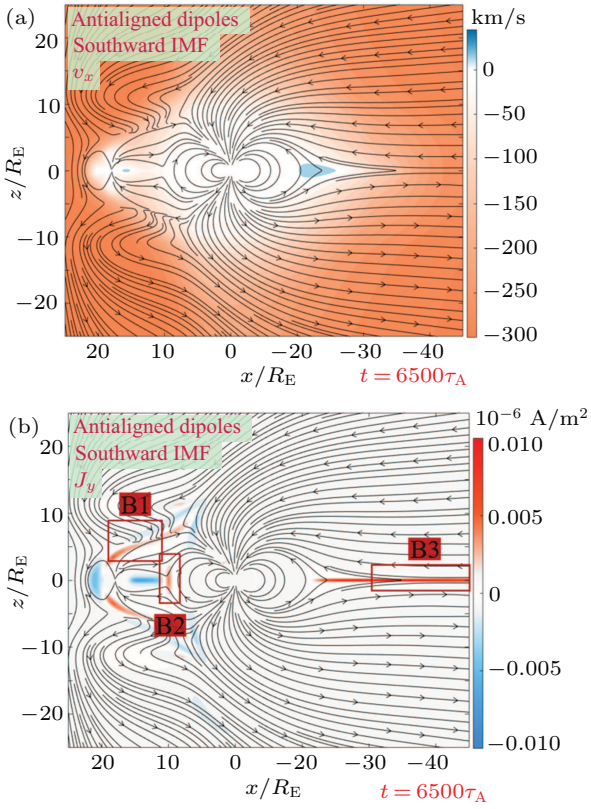


Fig. 6. QSS reconnection configurations in case noon, with antiparallel dipoles and southward IMFs. Magnetic field lines (in black) projection, as well as (a) x-component velocity v_x and (b) y-component current density J_y (both by color bars), are shown on the meridian plane.

In this case, unlike the case midnight, 3D features of reconnection configurations in the dayside are more significant. We then focus on the null pairs as a specific example. As observed by the Cluster spacecraft,[40,41] the null pair can be connected by a separator of the intersection of separatrices (called fans or Σ-surfaces) bounded by spines (γ-lines).[42,43] Taking region B1 marked in Fig. 6(b) for example, the null pair structure is exhibited in Fig. 7 with the antiparallel dipoles and the southward IMF for case noon. As shown in Fig. 7(a), a B–A–B null structure is formed in the lunar cusp region with the nulls (all on the meridian plane, $y = 0$, due to the symmetry) connected by an intersection (marked by a purple line in

Fig. 7(b)) of their fans. The fan of the A-type null (the green dot) is in green and that of the right B-type null (the orange dot) in Fig. 7(a) is in orange as shown in Fig. 7(b). Topologically, the fans Σ_A and Σ_B are bounded by the spines γ_B and γ_A respectively. And the structure connecting the left B-null and the A-null shows a similar structure. We then adopt $E_{\parallel} = \boldsymbol{E}\cdot\boldsymbol{B}/|\boldsymbol{B}|^2 \sim 10^{-19}$ at the midpoint of the separator to estimate the reconnection rate, which is nevertheless found to be much slower than that in X-line reconnection at subsolar point in case midnight.

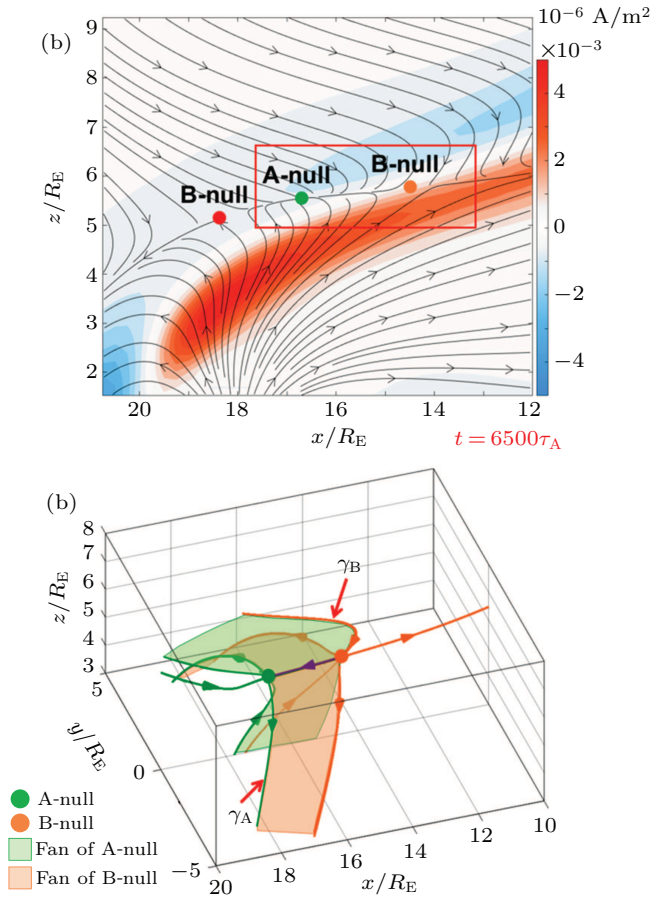


Fig. 7. (a) Local enlargement of Region B1 marked in Fig. 6(b); (b) 3D structure of A–B null pair inside red box in panel (a) and its fan.

Reconnection in the area between the Earth and the Moon, for case noon, is greatly influenced by the IMF orientation. For example, the reconnection (B2 marked in Fig. 6(b)) inflow, for the southward IMF, is almost in the x direction, while for the northward IMF, the reconnection inflow is almost in the z direction, similar to that in case midnight with both southward IMF and northward IMF. And for case noon with the parallel dipoles, reconnection occurs at lunar magnetopause, lunar cusp regions, Earth's cusp regions, or geomagnetotail according to various IMF orientations. Moreover, for the southward IMF, reconnection in the Earth's cusp region leads to an increase of the closed lunar magnetic flux while it has no influence on the lunar flux when the IMF orientation is northward. Besides, reconnection appears in the geomagnetotail for case noon with various dipole alignments and IMF orientations, similar to conventional geomagnetotail reconnection for today's geomagnetosphere, without the triple current sheets configuration.

We then summarize the reconnection processes and their features at different sites for case noon, with various dipole alignments and IMF orientations, in Tables 3 and 4.

Table 3. Antialigned dipoles at 12 LT.

IMF orientation	Reconnection site	Influences on the closed lunar magnetic flux
Southward	lunar cusp regions	
Southward	between Earth and Moon	decreasing
Southward	geomagnetotail	
Northward	lunar magnetopause	decreasing
Northward	between Earth and Moon	increasing
Northward	Earth's cusp regions	
Northward	geomagnetotail	

Table 4. Aligned dipoles at 12 LT.

IMF orientation	Reconnection site	Influences on the closed lunar magnetic flux
Southward	lunar magnetopause	decreasing
Southward	Earth's cusp regions	increasing
Southward	geomagnetotail	
Northward	lunar cusp regions	
Northward	Earth's cusp regions	
Northward	geomagnetotail	

3.3. Magnetic reconnection for Moon at 6-LT and 18-LT positions

Furthermore, the case for the Moon at the dawn side of the Earth at the 6-LT position (case dawn) is also investigated, while the case for the Moon positioning at the dusk side of the Earth (18 LT, case dusk) is symmetric to the former.

No or negligible reconnection is detected on the dawn side and dusk side of the Moon for case noon and case midnight. However, in case dawn/dusk, reconnection occurs not only at the magnetopause, magnetotail, and cusp regions of the Moon, but also notably on lunar dusk and dawn sides. The distributions of x-component current, J_x, on the dawn–dusk ($x = 0$) plane with different IMF orientations are shown in Fig. 8. For the southward IMF (Fig. 8(a)), a current sheet flowing along the x direction can be clearly observed between the Earth and the Moon (region A1), indicating magnetic flux transferring to the Moon by reconnection on the current sheet. And in the vicinity of the Moon, the high latitude current sheets symmetric about the equatorial ($z = 0$) plane can generate reconnection in the lunar cusp region. For the northward IMF (Fig. 8(b)), reconnection occurs at the dusk (region B1) side and the dawn (region B2) side of the Moon. The duskside (between the Earth and the Moon) reconnection rate is greatly weakened due to antialignment of the dipoles, while the dawnside reconnection rate is on the same order of magnitude as that of conventional X-line reconnection.

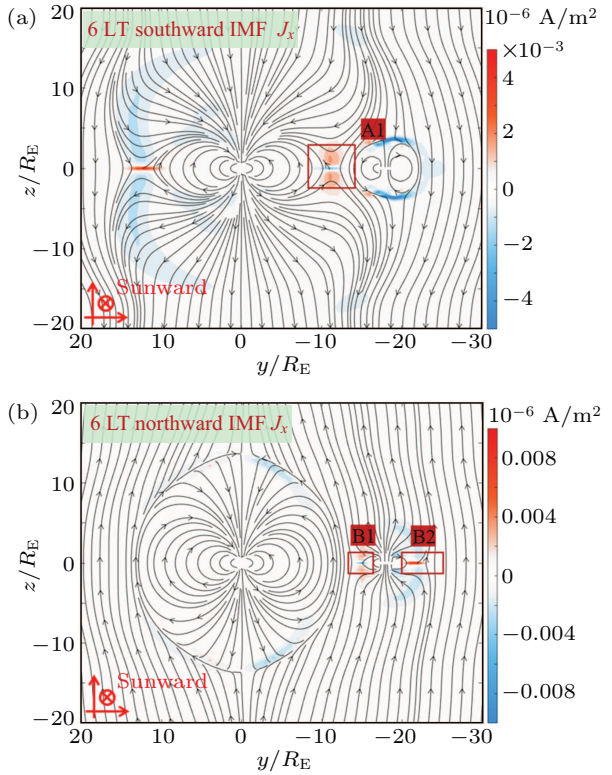


Fig. 8. QSS magnetic configurations with antiparallel dipoles at dawn–dusk cross-section $x = 0$. Patterns of magnetic field lines (in black) and x-component current J_x (denoted by color bar) are shown for (a) southward IMF and (b) northward IMF.

Table 5. Antialigned dipoles at 6 LT.

IMF orientation	Reconnection site	Influences on closed lunar magnetic flux
Southward	geomagnetopause	–
Southward	geomagnetotail	–
Southward	lunar cusp regions	–
Southward	lunar duskside	increasing
Northward	Earth's cusp regions	–
Northward	geomagnetotail	–
Northward	lunar magnetopause	decreasing
Northward	lunar magnetotail	increasing
Northward	lunar dawnside	increasing
Northward	lunar duskside	increasing

Table 6. Aligned dipoles at 6 LT.

IMF orientation	Reconnection site	Influences on closed lunar magnetic flux
Southward	geomagnetopause	–
Southward	geomagnetotail	–
Southward	lunar magnetopause	decreasing
Southward	lunar magnetotail	increasing
Southward	lunar dawnside	increasing
Southward	lunar duskside	increasing
Northward	Earth's cusp regions	–
Northward	geomagnetotail	–
Northward	lunar cusp regions	–

Besides, around the Earth in case dawn/dusk, the feature of reconnection on the meridian ($y = 0$) plane is very similar to that in conventional reconnection in today's geomagnetosphere. Nevertheless, such a kind of reconnection has almost no influence on the lunar flux transfer concerned.

Features of reconnection processes at various typical sites and their contributions to magnetic flux transports are then summarized in Tables 5 and 6. Due to the mirror symmetry, the contributions in case dusk are similar to those in case dawn.

4. Conclusions and perspectives

As a complex 3D system, the ancient solar–lunar terrestrial magneto-plasma system existing in the epoch when the Moon still possessed a global magnetic field substantially differs from the present-day geomagnetosphere. Specifically, the 3D magnetic reconnection process, magnetic configuration evolution of the ancient Earth–Moon–IMF system and corresponding reconnection dynamics are studied in a 3D MHD model with the various alignments of Earth–Moon dipoles and IMF orientations. The coupled quasi-steady-state magnetospheres are formed under different IMF conditions corresponding to various multiple X-points at various locations, including the geomagnetopause, the Earth's cusp region, the geomagnetotail, the lunar magnetopause, the lunar cusp region, the lunar magnetotail, and the area between the Earth and the Moon. Such geometries and processes can provide an effective pathway for facilitating the Earth-to-Moon transport of energy and materials, creating a possible mechanism and holding significant importance in understanding the origin and the evolution of the atmospheric and the soil constituents for coupled astrophysical systems with similar transport process.

Based on our research, there are three typical magnetic reconnection structures found in the simulation, i.e. the X-line, the triple current sheets, and the A–B null pair structures. The X-line structure occurs mostly in the area between the Earth and the Moon and the geomagnetopause with the southward IMF. The meridian cross-section of the X-line structure is a typical X-point geometry with a clearly inflow–outflow configuration. The A–B null pair structure appearing mainly at the lunar cusp region is more stable with a much lower reconnection rate than that for the X-line. The A-null and the B-null are linked by a separator line as an intersection of the fans (Σ-surfaces). Besides, a larger spatial scale magnetic reconnection structure is formed in the lunar magnetotail at 0 LT when the dipoles are antiparallel, with a triple current geometry of two reconnection currents along the $+y$ direction at the lunar cusp and the other aligning tail current in the $-y$ direction. Furthermore, for case dawn/dusk, reconnection on the lunar dusk side and dawn side may be significantly strengthened, thereby making a great influence on the closed lunar flux. The results of the complex multiple X-point configurations demonstrate a fresh and critical reconnection topology for 3D asymmetric system. With such a topology, the magnetic field line

configuration and the magnetic flux transfer process are different from the present-day Earth, offering a valuable idea for comprehending other asymmetrical coupled systems.

Therefore, based on our 3D MHD simulations, it can be proposed that magnetic reconnection may have a great influence on coupling and evolution of Moon–planet–IMF system and play a substantial role in their magnetic environments. For such astrophysical systems, the coupled magnetosphere can protect their ionospheres and atmospheres from eroding by high-energy particles and solar wind, resulting in a habitable environment that can lead to life. And on the other hand, as a key mechanism of the significant energy transfer process such as magnetosphere storms and substorms, the magnetic reconnection exhibits an intricate spatial configurations and temporal dynamics, potentially intensifying the extreme space weather events. For example, in the solar system, Jupiter, Saturn, and their major moons exhibit global magnetic fields,[44–46] indicating the possibility of analogously coupled magnetospheres and reconnection processes. Consequently, due to the existence of multiple X-point structures, some fast-growing events on these planets may show increasing complexity. Our work may also be of potential relevance in guiding the search for exoplanet life and the exploration of planets in the solar system. Further investigations for other dipole alignments and IMF orientations, as well as complex 3D reconnection geometries are subjects of future studies.

Acknowledgements

The authors thank Z. W. Ma and his team in the Institute for Fusion Theory and Simulation, Department of Physics, Zhejiang University, for providing the original 3D MHD code.

Project supported by the National Natural Science Foundation of China (Grant Nos. 11975087, 42261134533, and 42011530086), the National Magnetic Confinement Fusion Energy Research and Development Program of China (Grant No. 2022YFE03190400), and the Heilongjiang Touyan Innovation Team Program, China.

References

[1] Yamada M, Kulsrud R and Ji H T 2010 *Rev. Mod. Phys.* **82** 603
[2] Biskamp D 1996 *Astrophys. Space Sci.* **242** 165
[3] Zweibel E G and Yamada M 2009 *Annu. Rev. Astron. Astrophys.* **47** 291
[4] Priest E R and Forbes T. 1986 *J. Geophys. Res-Space Phys.* **91** 5579
[5] Pritchett P L 2001 *J. Geophys. Res-Space Phys.* **106** 3783
[6] Lu Q M, Fu H S, Wang R S and Lu S 2022 *Chin. Phys. B.* **31** 089401
[7] Comisso L and Bhattacharjee A 2016 *J. Plasma Phys.* **82** 595820601
[8] Birn J, Drake J F, Shay M A, Rogers B N, Denton R E, Hesse M, Kuznetsova M, Ma Z W, Bhattacharjee A, Otto A and Pritchett P L 2001 *J. Geophys. Res-Space Phys.* **106** 3715
[9] Liu Y H, Hesse M, Guo F, Daughton W, Li H, Cassak P A and Shay M A 2017 *Phys. Rev. Lett.* **118** 085101
[10] Torbert R B, Burch J L, Phan T D, *et al*. 2018 *Science* **362** 1391
[11] Burch J L, Torbert R B, Phan T D, *et al*. 2016 *Science* **352** aaf2939
[12] Lee L C and Fu Z F 1986 *J. Geophys. Res-Space Phys.* **91** 6807
[13] Wang Z X, Wang X G, Dong J Q, Lei Y A, Long Y X, Mou Z Z and Qu W X 2007 *Phys. Rev. Lett.* **99** 185004
[14] Pontin D I 2011 *Adv. Space Res.* **47** 1508
[15] Guo R, Pu Z, Wang X, Xiao C and He J 2022 J *J. Geophys. Res-Space Phys.* **127** e2021JA030248
[16] Xiao C J, Wang X G, Pu Z Y, Ma Z W, Zhao H, Zhou G P, Wang J X, Kivelson M G, Fu S Y, Liu Z X, Zong Q G, Dunlop M W, Glassmeier K H, Lucek E, Reme H, Dandouras I and Escoubet C P 2007 *Nat. Phys.* **3** 609
[17] Hale G E 1908 *ApJ* **28** 315
[18] Beck R 2001 *Space Sci. Rev.* **99** 243
[19] Zweibel E G and Heiles C 1997 *Nature* **385** 131
[20] Lu Q M, Guo J, Lu S, Wang X Y, Slavin J A, Sun W J, Wang R S, Lin Y and Zhong J 2022 *ApJ* **937** 1
[21] Ferrari C, Govoni F, Schindler S, Bykov A M and Rephaeli Y 2008 *Space Sci. Rev.* **134** 93
[22] Ryu D, Schleicher D R, Treumann R A, Tsagas C G and Widrow L M 2012 *Space Sci. Rev.* **166** 1
[23] Ji H, Yoo J, Fox W, Yamada M, Argall M, Egedal J, Liu Y H, Wilder R, Eriksson S, Daughton W, Bergstedt K, Bose S, Burch J, Torbert R, Ng J and Chen L J 2023 *Space Sci. Rev.* **219** 76
[24] Mitchell D L, Halekas J S, Lin R P, Frey S, Hood L L, Acuña M H and Binder A 2008 *Icarus* **194** 401
[25] Mighani S, Wang H, Shuster D L, Borlina C S, Nichols C I and Weiss B P 2020 *Sci. Adv.* **6** eaax0883
[26] Zharkov V N 2000 *Solar System Res.* **34** 1
[27] Green J, Draper D, Boardsen S and Dong C 2020 *Sci. Adv.* **6** eabc0865
[28] Bingert S and Peter H 2011 *Astron. Astrophys.* **530** A112
[29] Groth C P, De Zeeuw, D L, Gombosi T I and Powell K G 2000 *J. Geophys. Res-Space Phys.* **105** 25053
[30] Ogino T A 1986 *J. Geophys. Res-Space Phys.* **91** A6
[31] Tanaka T 1995 *J. Geophys. Res-Space Phys.* **100** A7
[32] Dorelli J C and Bhattacharjee A 2008 *Phys. Plasmas* **15** 056504
[33] Li L 2021 *AIP Adv.* **4** 11
[34] Cranmer S R 2017 *ApJ* **840** 114
[35] Gold T 1959 *J. Geophys. Res.* **64** 1219
[36] Parker E N 1957 *J. Geophys. Res.* **62** 509
[37] Petschek H E 1964 *NASA Spec Publ.* 425
[38] Dahlburg R B and Karpen J T 1995 *J. Geophys. Res-Space Phys.* **100** A12
[39] Wei L, Yu F and Wang Z X 2020 *Phys. Plasmas* **27** 012103
[40] Xiao C J, Wang X G, Pu Z Y, Zhao H, Wang J X, Ma Z W, Fu S Y, Kivelson M G, Liu Z X, Zong Q G, Glassmeier K H, Balogh A, Korth A, Reme H and Escoubet C P 2006 *Nat. Phys.* **2** 478
[41] Xiao C J, Wang X G, Pu Z Y, Ma Z W, Zhao H, Zhou G P, Wang J X, Kivelson M G, Fu S Y, Liu Z X, Zong Q G, Dunlop M W, Glassmeier K H, Lucek E, Reme H, Dandouras I and Escoubet C P 2007 *Nat. Phys.* **3** 609
[42] Lau Y T and Finn J M 1990 *ApJ* **350** 672
[43] Greene J M 1988 *J. Geophys. Res-Space Phys.* **93** 8583
[44] Gastine T, Wicht J, Duarte L D V, Heimpel M and Becker A 2014 *Geophys. Res. Lett.* **41** 5410
[45] Acuña M H, Ness N F and Connerney J E P 1980 *J. Geophys. Res-Space Phys.* **85** 5675
[46] Jia X, Kivelson M G, Khurana K K and Walker R J 2010 *Space Sci. Rev.* **152** 271